



**HAL**  
open science

## **Electrodeposition of HAp coatings on Ti6Al4V alloy and its electrochemical behavior in simulated body fluid solution**

Thi Mai Thanh Dinh, Thi Thom Nguyen, Thi Nam Pham, Thu Phuong Nguyen, Thi Thu Trang Nguyen, Thai Hoang, David Grossin, Ghislaine Bertrand, Christophe Drouet

### ► To cite this version:

Thi Mai Thanh Dinh, Thi Thom Nguyen, Thi Nam Pham, Thu Phuong Nguyen, Thi Thu Trang Nguyen, et al.. Electrodeposition of HAp coatings on Ti6Al4V alloy and its electrochemical behavior in simulated body fluid solution. *Advances in Natural Sciences: Nanoscience and Nanotechnology*, 2016, 7 (2), pp.1-8. 10.1088/2043-6262/7/2/025008 . hal-02430135

**HAL Id: hal-02430135**

**<https://hal.science/hal-02430135>**

Submitted on 7 Jan 2020

**HAL** is a multi-disciplinary open access archive for the deposit and dissemination of scientific research documents, whether they are published or not. The documents may come from teaching and research institutions in France or abroad, or from public or private research centers.

L'archive ouverte pluridisciplinaire **HAL**, est destinée au dépôt et à la diffusion de documents scientifiques de niveau recherche, publiés ou non, émanant des établissements d'enseignement et de recherche français ou étrangers, des laboratoires publics ou privés.



## Open Archive Toulouse Archive Ouverte (OATAO)

OATAO is an open access repository that collects the work of Toulouse researchers and makes it freely available over the web where possible

This is a Publisher's version published in: <http://oatao.univ-toulouse.fr/24462>

**Official URL:** <https://doi.org/10.1088/2043-6262/7/2/025008>

### **To cite this version:**

Dinh, Thi Mai Thanh and Nguyen, Thi Thom and Pham, Thi Nam and Nguyen, Thu Phuong and Nguyen, Thi Thu Trang and Hoang, Thai and Grossin, David  and Bertrand, Ghislaine  and Drouet, Christophe   
*Electrodeposition of HAp coatings on Ti6Al4V alloy and its electrochemical behavior in simulated body fluid solution.* (2016) *Advances in Natural Sciences: Nanoscience and Nanotechnology*, 7 (2). 1-8. ISSN 2043-6254

Any correspondence concerning this service should be sent to the repository administrator: [tech-oatao@listes-diff.inp-toulouse.fr](mailto:tech-oatao@listes-diff.inp-toulouse.fr)

# Electrodeposition of HAp coatings on Ti6Al4V alloy and its electrochemical behavior in simulated body fluid solution

Thi Mai Thanh Dinh<sup>1</sup>, Thi Thom Nguyen<sup>1</sup>, Thi Nam Pham<sup>1</sup>,  
Thu Phuong Nguyen<sup>1</sup>, Thi Thu Trang Nguyen<sup>1</sup>, Thai Hoang<sup>1</sup>,  
David Grossin<sup>2</sup>, Ghislaine Bertrand<sup>2</sup> and Christophe Drouet<sup>2</sup>

<sup>1</sup> Institute for Tropical Technology, Vietnam Academy of Science and Technology, 18 Hoang Quoc Viet Street, Cau Giay, Hanoi, Vietnam

<sup>2</sup> CIRIMAT Carnot Institute, UMR CNRS/UPS/INPT 5085, University of Toulouse, ENSIACET, 4 allée Emile Monso, F-31030 Toulouse cedex 4, France

E-mail: dmthanh@itt.vast.vn

Received 28 January 2016

Accepted for publication 24 March 2016

Published 22 April 2016



CrossMark

## Abstract

Hydroxyapatite (HAp) coatings were prepared on Ti6Al4V substrate by electrodeposition method from electrolyte solution containing  $\text{Ca}(\text{NO}_3)_2$ ,  $\text{NH}_4\text{H}_2\text{PO}_4$  and  $\text{NaNO}_3$ . The results show that the HAp coatings were single phase crystals of HAp. Scanning electron microscope (SEM) images present that HAp/Ti6Al4V have flake shapes which arrange to form like-coral agglomerates. *In vitro* test of the Ti6Al4V and HAp/Ti6Al4V in simulated body fluid (SBF) solution was investigated with different immersion times. pH of SBF solution decreased and the mass of materials increased. SEM images prove the formation of apatite on the surface of Ti6Al4V and HAp/Ti6Al4V. The corrosion current density during immersion time of substrate is always higher than the one of HAp/Ti6Al4V because the deposited HAp can protect well for the substrate.

Keywords: Ti6Al4V, electrodeposition, HAp, SBF

Classification numbers: 2.03, 4.02

## 1. Introduction

In humans and mammals, hydroxyapatite (HAp,  $\text{Ca}_{10}(\text{PO}_4)_6(\text{OH})_2$ ) is the main component of bone and teeth. Synthetic HAp has similar chemical composition, crystal structure and high biocompatibility as the natural bone tissue [1, 2]. It has bioactive and high biocompatibility with cells, tissues and can create direct bonding with immature bone. The result is the quick regeneration of bone. Thus HAp is used as a popular material for bone and tooth implants in the biomaterial field. However, the mechanical strength of HAp is too low to be used in any load-bearing applications. For

exploiting the biocompatibility of HAp in the fabrication of bone and tooth implants it was coated on metal or alloy: Ti, 316L stainless steel, CoCrMoNi, TiN,  $\text{TiO}_2$ , Ti6Al4V etc. HAp coatings can be synthesized by many different methods such as: electrophoretic deposition [3, 4], plasma spraying [5, 6], sol-gel [7, 8], biomimetic deposition [9] and electrodeposition [1, 9, 10]. Among the above methods, electrodeposition is one of the most promising methods to synthesize thin HAp coatings.

Ti6Al4V is a common metallic alloy which has found many uses as biomaterials in the human body. It has been increasingly preferred in the biomedical arena with cardiovascular, dental and orthopedic applications because of their properties. Titanium (Ti) and its alloy (Ti6Al4V) are metallic materials commonly employed as orthopedic implants because of their high strength (compared with polymeric materials) and high toughness (compared with ceramic

 Original content from this work may be used under the terms of the Creative Commons Attribution 3.0 licence. Any further distribution of this work must maintain attribution to the author(s) and the title of the work, journal citation and DOI.

**Table 1.** Elemental content of Ti6Al4V alloy.

Element	Ti	Al	V	C	Fe
Content (%)	89.63	6.04	4.11	0.05	0.17

materials) [11]. However, metallic materials are susceptible to corrosive attack by body fluids. Problems such as release of inflammatory mediators might cause adverse effects to the surrounding tissues [12]. Moreover, metallic surfaces are in general not adequately bioactive. Therefore, to improve osteo-integration with bone tissues, many researchers synthesized HAp coatings on the surface of metals or alloys. Some studies indicated that HAp coatings on substrates have good biocompatibility when they were immersed in simulated body fluid (SBF) solution and HAp coatings on substrates are bioactive materials for biomedical applications [13–16].

In this work we electrodeposited HAp coatings on Ti6Al4V with the variation of scanning potential range and scan number. Then electrochemical behaviors of Ti6Al4V and HAp/Ti6Al4V materials were investigated in SBF solution.

## 2. Materials and methods

### 2.1. Materials

The HAp coatings were electrodeposited on Ti6Al4V bio-metallic alloy with the elemental compositions given in table 1. A coupon of Ti6Al4V ( $1.5 \times 1 \times 0.2 \text{ cm}^3$ ) was used as a cathode (working electrode) for the experiments. Prior to electrodeposition, the cathode was polished with SiC papers (ranging from P320 to P1200 grit), followed by ultrasonic rinsing in distilled water for 15 min and then dried at room temperature. The electrode working area was  $1 \text{ cm}^2$ .

The chemicals were used for the experiments: calcium nitrate tetrahydrate ( $\text{Ca}(\text{NO}_3)_2 \cdot 4\text{H}_2\text{O}$ ,  $M = 236.15 \text{ g mol}^{-1}$ , 99% pure), ammonium dihydrogen phosphate ( $\text{NH}_4\text{H}_2\text{PO}_4$ ,  $M = 115.03 \text{ g mol}^{-1}$ , pure 99%) and sodium nitrate ( $\text{NaNO}_3$ ,  $M = 84.99 \text{ g mol}^{-1}$ , 99% pure) were imported from China.

### 2.2. Electrodeposition

The electrolyte solution contained 30 mM  $\text{Ca}(\text{NO}_3)_2$ , 18 mM  $\text{NH}_4\text{H}_2\text{PO}_4$  and 60 mM  $\text{NaNO}_3$  with the ratio of Ca/P being 1.67 dissolved in distilled water. The presence of  $\text{NaNO}_3$  in the electrolyte solution increases the ionic strength of the electrolyte and for potentially exploiting the electrochemical reduction of  $\text{NO}_3^-$  ions which contributes to generate  $\text{OH}^-$  [17, 18]. The pH of the electrolyte solution was 4.4.

HAp coatings were synthesized in a cell containing 80 ml of the above electrolyte solution with three electrodes: the working electrode was a Ti6Al4V sheet; a Pt foil was used as counter electrode (anode) and a Hg/Hg<sub>2</sub>Cl<sub>2</sub>/KCl (SCE) electrode was used as reference. The deposition temperature was adjusted at 50 °C by a thermostat (VELP, Italia).

**Table 2.** Chemical composition of the SBF solution.

Compound	Content ( $\text{g l}^{-1}$ )
NaCl	8.00
KCl	0.40
CaCl <sub>2</sub>	0.18
NaHCO <sub>3</sub>	0.35
Na <sub>2</sub> HPO <sub>4</sub> · 2H <sub>2</sub> O	0.48
MgCl <sub>2</sub> · 6H <sub>2</sub> O	0.10
KH <sub>2</sub> PO <sub>4</sub>	0.06
MgSO <sub>4</sub> · 7H <sub>2</sub> O	0.10
Glucose	1.00

The electrodeposition was carried out using an Autolab with different synthesis conditions: scanning potential ranges: 0 to  $-1.8$ ; 0 to  $-1.9$ ; 0 to  $-2.0$ ; 0 to  $-2.2$  and 0 to  $-2.5 \text{ V/SCE}$ ; scan numbers: 1, 3, 5, 7 and 10 scans. HAp coatings were lightly rinsed by distilled water. Then they were dried at the room temperature.

### 2.3. Coating characterization

Molecular structure of HAp coating was determined by Fourier transform infrared spectroscopy (FTIR 6700, Nicolet) using KBr pellet technique at room temperature, in the range from 400 to  $4000 \text{ cm}^{-1}$  with  $16 \text{ cm}^{-1}$  resolution and 16 scans signal average. HAp coatings were lightly separated from the substrate and the phase structure of HAp coatings were characterized by x-ray diffraction (XRD) (Siemen D5005 Bruker-Germany, Cu-K $\alpha$  radiation ( $\lambda = 1.5406 \text{ \AA}$ )), operated at 40 kV and 30 mA, with step angle of  $0.030^\circ \text{ s}^{-1}$  and in a  $2\theta$  degree range of  $20^\circ$ – $50^\circ$ . The average crystallite size along  $c$ -direction of electrodeposited HAp was calculated from (002) reflection in XRD pattern, using Scherrer's equation:

$$D = \frac{0.9\lambda}{B \cos \theta}, \quad (1)$$

where  $D$  (nm) is crystallite size,  $\lambda$  (nm) is the wavelength of the radiation,  $\theta$  (rad) is the diffraction angle and  $B$  is the full-width at half-maximum of the peak along (002) direction

Surface morphology of HAp coatings before and after immersion in the SBF solution were examined using a Hitachi S-4800 scanning electron microscope (SEM). HAp coating thickness was determined following ISO 4288-1998 standard by the Alpha-Step IQ equipment (KLA-Tencor-USA). The coating thickness is the average value of five measurements.

### 2.4. In vitro test

A liter of the SBF solution was prepared by dissolution of chemicals in distilled water (table 2). The pH of the SBF solution was adjusted to 7.4 by 1 M HCl solution and the temperature was maintained at 37 °C by water bath [19–21].

Ti6Al4V and HAp/Ti6Al4V materials were limited to  $1 \text{ cm}^2$  of active area and they were immersed in Falcon tubes containing 40 ml of the SBF solution at 37 °C in a water bath for 1, 5, 7, 11, 14 and 21 days. The electrochemical behavior of the materials was tested by Autolab equipment with a three

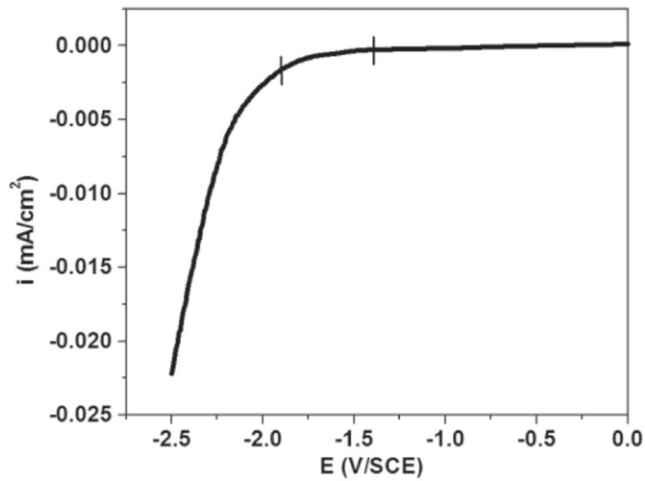


**Figure 1.** The cathodic polarization curve of Ti6Al4V electrode in the electrolyte solution: 30 mM Ca(NO<sub>3</sub>)<sub>2</sub>, 18 mM NH<sub>4</sub>H<sub>2</sub>PO<sub>4</sub> and 60 mM NaNO<sub>3</sub>.

electrodes cell. The above materials were used as working electrode, a saturated calomel electrode (SCE) as a reference electrode and Pt foil as a counter electrode.

The working electrode was polarized in the potential range of ±10 mV around its open circuit potential (OCP) with a scan rate of 1 mV s<sup>-1</sup>. From polarization curves Δ*E*, Δ*I* values were determined. The polarization resistance *R*<sub>p</sub> and the corrosion current density *i*<sub>corr</sub> were calculated from equations

$$R_p = \frac{\Delta E}{\Delta i}, \quad (2)$$

$$i_{\text{corr}} = \frac{B}{R_p}, \quad (3)$$

the *B* values were determined from the Tafel slopes of *i*-*E* curves in the potential range OCP ± 100 mV with a scan rate of 1 mV s<sup>-1</sup> by using equation

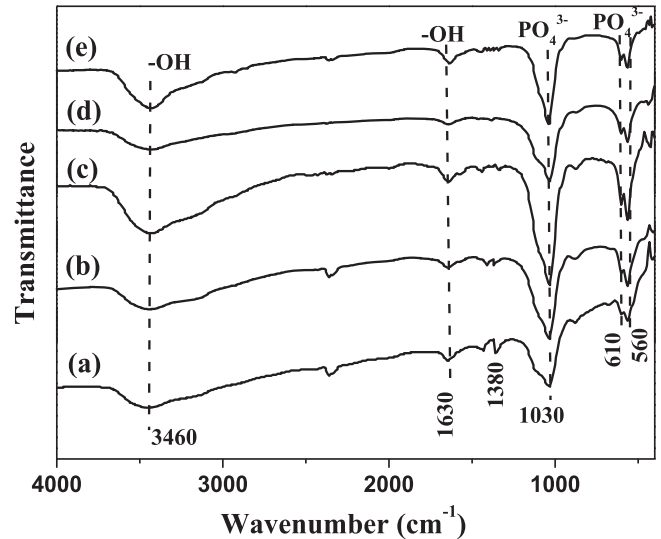
$$B = \frac{b_a |b_c|}{2.3(b_a + |b_c|)}, \quad (4)$$

where *b*<sub>a</sub> is the value of the anodic Tafel slope and |*b*<sub>c</sub>| is the absolute value of the cathodic Tafel slope. We obtain *B* = 0.01426 and 0.0119 corresponding to Ti6Al4V and HAp/Ti6Al4V.

### 3. Results and discussions

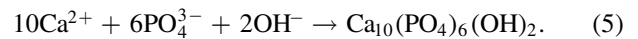
#### 3.1. The cathodic polarization curve of Ti6Al4V

Figure 1 shows the cathodic polarization curve of Ti6Al4V substrate in the above electrolyte at the scanning potential range from 0 to -2.5 V/SCE with a scan rate of 5 mV s<sup>-1</sup> at 50 °C. The cathodic polarization curve has similar shape and consistent with the reported results [16, 21]. In this scanning range there is reduction of O<sub>2</sub>, H<sub>2</sub>PO<sub>4</sub><sup>-</sup>, HPO<sub>4</sub><sup>2-</sup> and H<sub>2</sub>O to create PO<sub>4</sub><sup>3-</sup> and OH<sup>-</sup>. The OH<sup>-</sup> and PO<sub>4</sub><sup>3-</sup> react with Ca<sup>2+</sup> ions to form HAp coatings on the cathode according to the

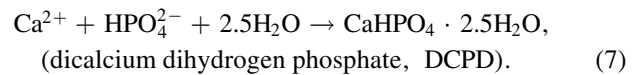
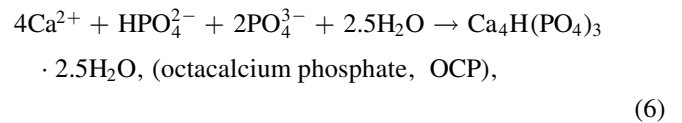


**Figure 2.** FTIR spectra of HAp synthesized on Ti6Al4V with the different scanning potential ranges (a) 0 to -1.8 (b) 0 to -1.9 (c) 0 to -2.0 (d) 0 to -2.2 and (e) 0 to -2.5.

chemical reaction



Beside, different compounds of Ca and P are results of following reactions:



#### 3.2. Effect of scanning potential range

Based on the analysis of the cathodic polarization curve, HAp coating was electrodeposited in the electrolyte solution (pH = 4.4) with different scanning potential ranges: from 0 to -1.8; 0 to -1.9; 0 to -2.0; 0 to -2.2 and 0 to -2.5 V/SCE during 5 scans with a scan rate of 5 mV s<sup>-1</sup>, at 50 °C.

FTIR spectra of HAp synthesized on the surface of Ti6Al4V with different scanning potential ranges are presented in figure 2. All of the spectra show the characteristic bands of PO<sub>4</sub><sup>3-</sup> group (asymmetric stretching vibration of P-O bond at 1030 cm<sup>-1</sup>; asymmetric O-P-O bending mode at 560 cm<sup>-1</sup>). Absorption peaks at 3460 and 610 cm<sup>-1</sup> usually assigned to the O-H stretching vibration in hydroxyapatite were not clearly distinguished on these spectra. This can be explained by the non-stoichiometry of the apatite phase, with a deficiency in calcium and hydroxide groups. Water bands were visible by a large band in the range 3460 cm<sup>-1</sup> (O-H stretching from water molecules) and by the H-O-H bending band at 1630 cm<sup>-1</sup>. Beside, the presence of peak in the region around 1380 cm<sup>-1</sup> can be assigned to the vibration modes of

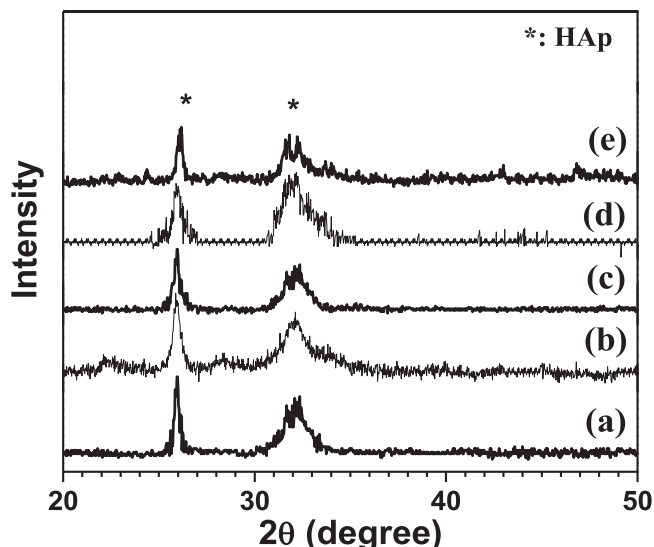


**Figure 3.** XRD patterns of HAp synthesized on Ti6Al4V with the different scanning potential ranges (a) 0 to  $-1.8$  (b) 0 to  $-1.9$  (c) 0 to  $-2.0$  (d) 0 to  $-2.2$  and (e) 0 to  $-2.5$ .

$\text{CO}_3^{2-}$ . The occurrence of  $\text{CO}_3^{2-}$  may be due to the reaction of atmospheric  $\text{CO}_2$  with  $\text{OH}^-$  ions, hence the content of  $\text{CO}_3^{2-}$  ions is rather low [16].

Figure 3 presents the XRD diffraction patterns of HAp synthesized on the surface of Ti6Al4V in  $2\theta$  of  $20^\circ$ – $50^\circ$ . The XRD patterns only exhibit the hydroxyapatite phase (denoted \* in figure 3). The typical peaks are found at  $2\theta \approx 26^\circ$  and  $32^\circ$  corresponding to (002) and (211) planes.

The HAp crystal diameter calculated from the Scherrer equation shows that the crystals have nano-size (89–106 nm). The crystal diameter changes not much when the potential range changes from 0 to  $-1.8$  V/SCE to 0 to  $-2.0$  V/SCE. However, with the larger potential range the crystal diameter increases significantly (table 3). It can be explained as following: with the large potential range, much  $\text{OH}^-$ ,  $\text{PO}_4^{3-}$  ions were generated leading to the large formation of HAp; the HAp particles concentrated to form larger particles.

The SEM images of HAp coatings on Ti6Al4V were shown in figure 4. The results show that with the different potential ranges, the surface morphology does not change. All of the samples, the substrates were covered completely by HAp coatings. At low magnification the crystals of HAp have coral-like shape. At high magnification, SEM images clearly show that HAp crystals have flake-like shape to form coarse granular agglomerates.

Table 4 showed the thickness of HAp coatings synthesized with different potential ranges. The coating thickness increases and reaches a maximum value at  $7.91 \mu\text{m}$  (the potential range 0 to  $-2.0$  V/SCE, respectively). When the potential range was larger, the thickness of HAp coatings

decreases. The coating thickness is  $4.68 \mu\text{m}$  with the potential range from 0 to  $-2.5$  V/SCE. The decrease of the coating thickness can be explained as following: with the large scanning potential range, the further increase in the amount of  $\text{OH}^-$  and  $\text{PO}_4^{3-}$  ions on the electrode surface, leading to their diffusion from the electrode surface into the solution and these ions combined with  $\text{Ca}^{2+}$  to form HAp in the solution. Simultaneously, with the large cathode potential, the reduction of water is promoted, thus the hydrogen bubbles are created on the electrode surface that may reduce adhesion ability of HAp coatings with Ti6Al4V substrate. So the suitable potential range is 0 to  $-2.0$  V/SCE.

### 3.3. Effect of scan number

Deposition time affects the thickness and surface morphology of HAp coatings. We electrodeposited HAp coatings in the potential range 0 to  $-2.0$  V/SCE with the change of scan number: 1, 3, 5, 7 and 10 scans with constant scan rate ( $5 \text{ mV s}^{-1}$ ). SEM images of the HAp coatings on the surface of Ti6Al4V are shown in figure 5. With different scan number, the morphology of HAp coatings is various. It is explained as following: with change of scan number,  $\text{OH}^-$ ,  $\text{PO}_4^{3-}$  ions are differently formed and they affect the formation and crystallization of HAp.

Table 5 presents the HAp coating thickness synthesized with the different scan numbers. The coating thickness increases and reaches the maximum value after 5 scans. The scan number increases continually, the thickness of HAp coatings decreases due to peeling of HAp coatings. Therefore, 5 scans was chosen to synthesize HAp coatings on Ti6Al4V by electrodeposition method. In the next parts, we synthesized HAp/Ti6Al4V at condition: the potential range from 0 to  $-2.0$  V/SCE; 5 scans;  $5 \text{ mV s}^{-1}$  at  $50^\circ\text{C}$  to investigate *in vitro* test.

### 3.4. In vitro test

The electrochemical behaviors of Ti6Al4V and HAp/Ti6Al4V materials in the SBF solution were also investigated.

**3.4.1. The variation of pH solution.** Figure 6 shows the pH values of the SBF solutions containing Ti6Al4V and HAp/Ti6Al4V materials with different immersion times at  $37^\circ\text{C}$ . The pH value of the SBF solution before soaking is 7.4. The pH of the SBF solutions decreased during the immersion time. Moreover, the pH of SBF solution containing HAp/Ti6Al4V decreases more strongly in comparison with Ti6Al4V substrate. It can be hypothesized that HAp as nucleation promotes the formation of apatite. The formation of apatite consumed  $\text{OH}^-$  leading to the reduction of pH solution, the pH solution

**Table 3.** The crystal diameter of HAp electrodeposited with the different potential ranges.

Potential range (V/SCE)	0 to $-1.8$	0 to $-1.9$	0 to $-2.0$	0 to $-2.2$	0 to $-2.5$
Crystal diameter (nm)	89	89	90	106	106

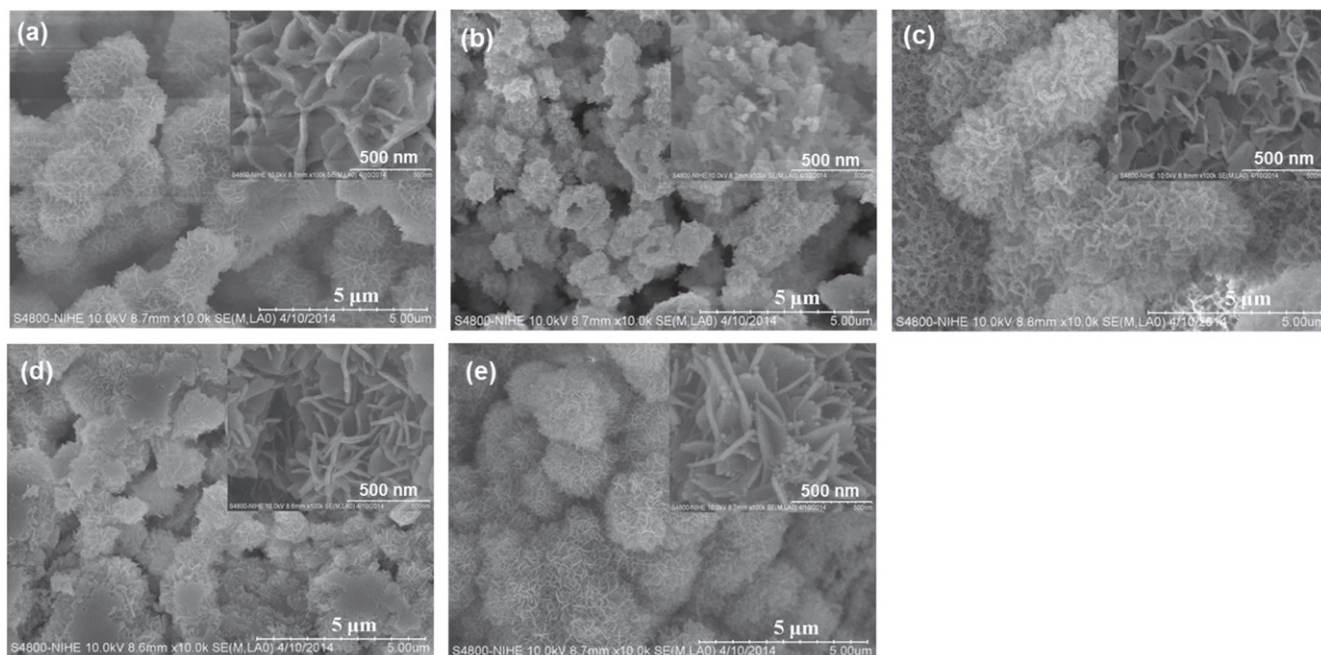


**Figure 4.** SEM images of HAp/Ti6Al4V synthesized with the different potential ranges: (a) 0 to -1.8, (b) 0 to -1.9, (c) 0 to -2.0, (d) 0 to -2.2 and (e) 0 to -2.5 V/SCE.

**Table 4.** The thickness of HAp coatings synthesized with the different potential ranges.

The potential range (V/SCE)	0 to -1.8	0 to -1.9	0 to -2.0	0 to -2.2	0 to -2.5
The thickness ( $\mu\text{m}$ )	$4.9 \pm 0.3$	$6.0 \pm 0.2$	$7.9 \pm 0.2$	$5.98 \pm 0.3$	$4.7 \pm 0.4$

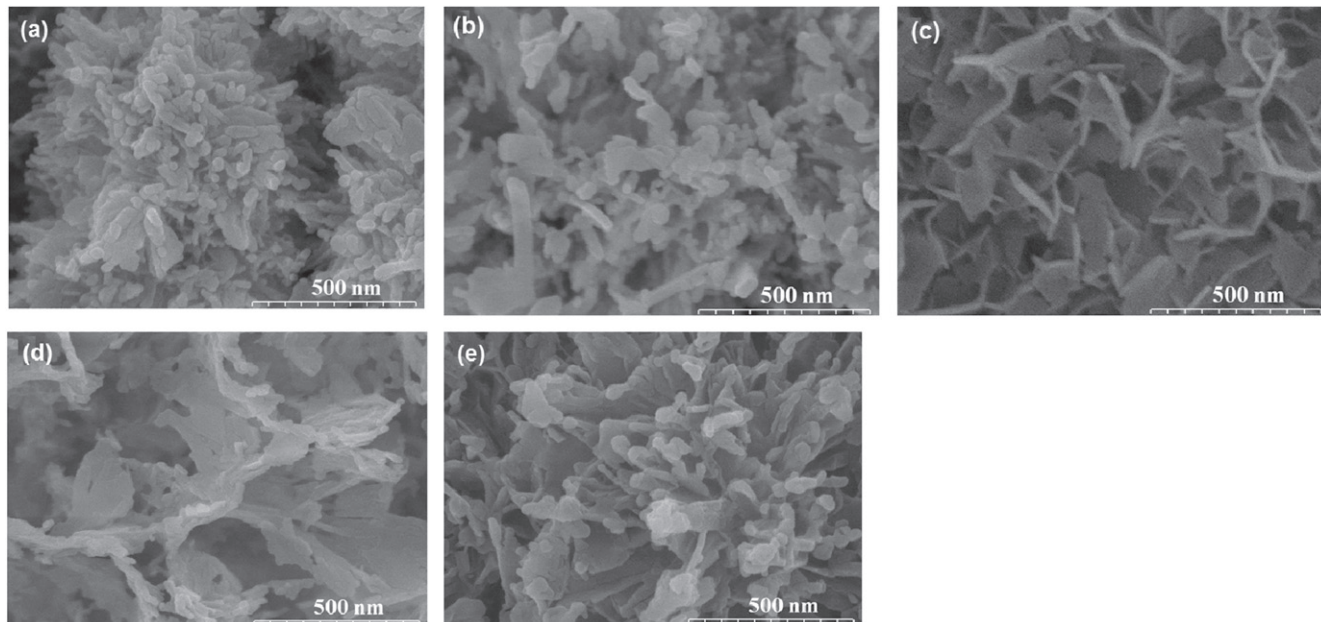


**Figure 5.** SEM images of HAp coatings with the different scan numbers: (a) 1; (b) 3; (c) 5; (d) 7 and (e) 10 scans.

**Table 5.** The thickness of HAp coatings synthesized with the different scan numbers.

The scan number	1	3	5	7	10
The thickness ( $\mu\text{m}$ )	$2.0 \pm 0.2$	$5.5 \pm 0.2$	$7.9 \pm 0.2$	$6.4 \pm 0.3$	$5.3 \pm 0.4$

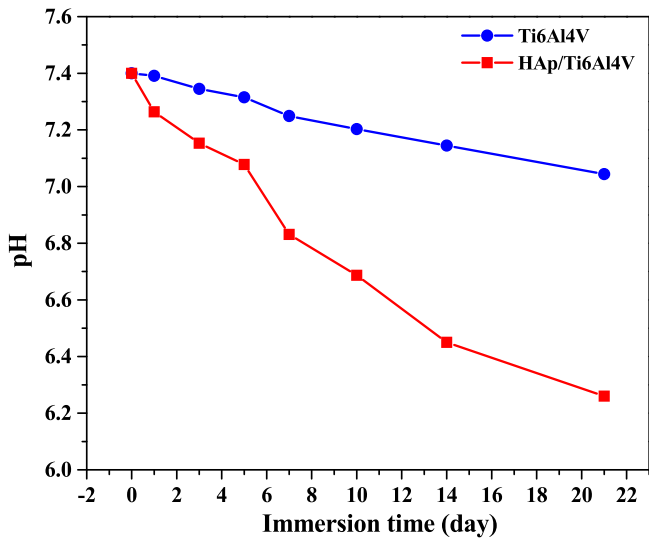


Figure 6. The pH value of SBF solution immersed Ti6Al4V and HAp/Ti6Al4V materials versus different immersion times at 37 °C.

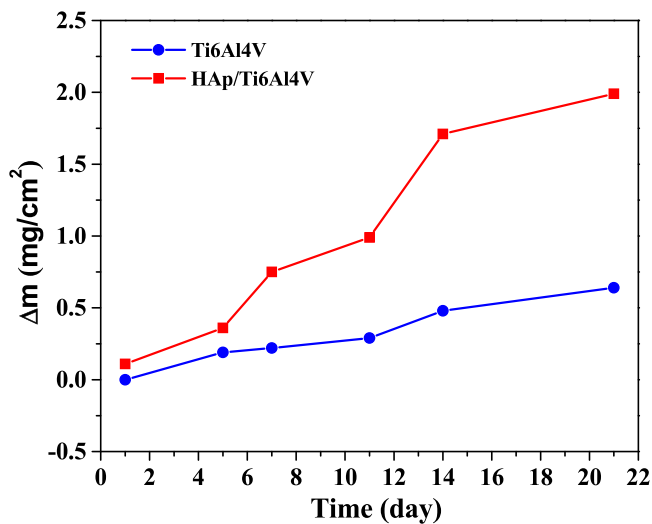


Figure 7. The mass variation of Ti6Al4V and HAp/Ti6Al4V versus different immersion times in the SBF solution.

containing HAp/Ti6Al4V decreases strongly during immersion time. This result shows that the formation of apatite was significant. After 21 immersion days in the SBF

solution, the pH value of the solution immersed HAp/Ti6Al4V was 6.16.

3.4.2. *Variation of mass.* The mass variation of Ti6Al4V and HAp/Ti6Al4V materials with different immersion times is displayed in figure 7. The mass of Ti6Al4V substrate during immersion time changed not much. After 21 immersion days in the SBF solution, the mass of Ti6Al4V is 0.08 mg cm<sup>-2</sup>. With HAp/Ti6Al4V, the mass of material increased during the immersion process. After 21 immersion days the mass variation of HAp/Ti6Al4V is 1.99 mg cm<sup>-2</sup>. It is clear that the formation of apatite crystals on the surface of material increased significantly. These results are confirmed by the SEM images (figures 8 and 9).

3.4.3. *The SEM images.* Figures 8 and 9 display SEM images of Ti6Al4V and HAp/Ti6Al4V materials before and after immersion in the SBF solution with different times. The SEM image of the Ti6Al4V sample after 21 immersion days in the SBF solution observed the formation of apatite crystals. However apatite crystals do not cover substrate fully (figure 8).

HAp coatings on Ti6Al4V have flake-like shape to form coarse granular agglomerates before immersed in the SBF solution. After immersion in SBF solution, morphology has clear change. It shows the formation of apatite crystals on the surface of HAp/Ti6Al4V. The apatite crystals are observed with cylinder shape and clump to form groups with cactus shape. Specially, with the sample immersed during 21 days in the SBF solution, apatite crystals grew up to form a thicker block on the surface of material. The results about the formation of apatite crystals are suitable with decrease of pH and increase of sample mass in the immersion process. These materials exhibit good biocompatibility in the SBF solution.

3.4.4. *Polarization measurements.* Variation of parameters  $E_{corr}$ ,  $i_{corr}$ ,  $R_p$  according to immersion time was calculated from polarization potential measurements results of Ti6Al4V and HAp/Ti6Al4V materials in the SBF solution (table 6). The variation of  $i_{corr}$  as well as  $R_p$  is not following a rule, these values fluctuate at different immersion times. After 1 immersed day in SBF solution, polarization resistance  $R_p$  of HAp/Ti6Al4V is much higher than that of Ti6Al4V (60.7

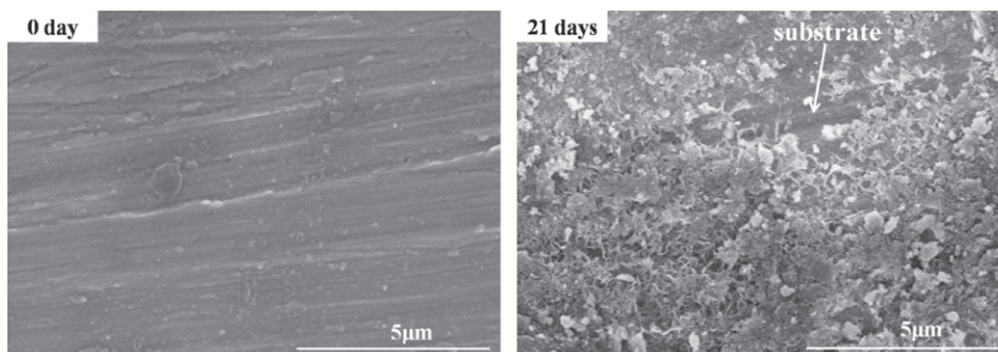
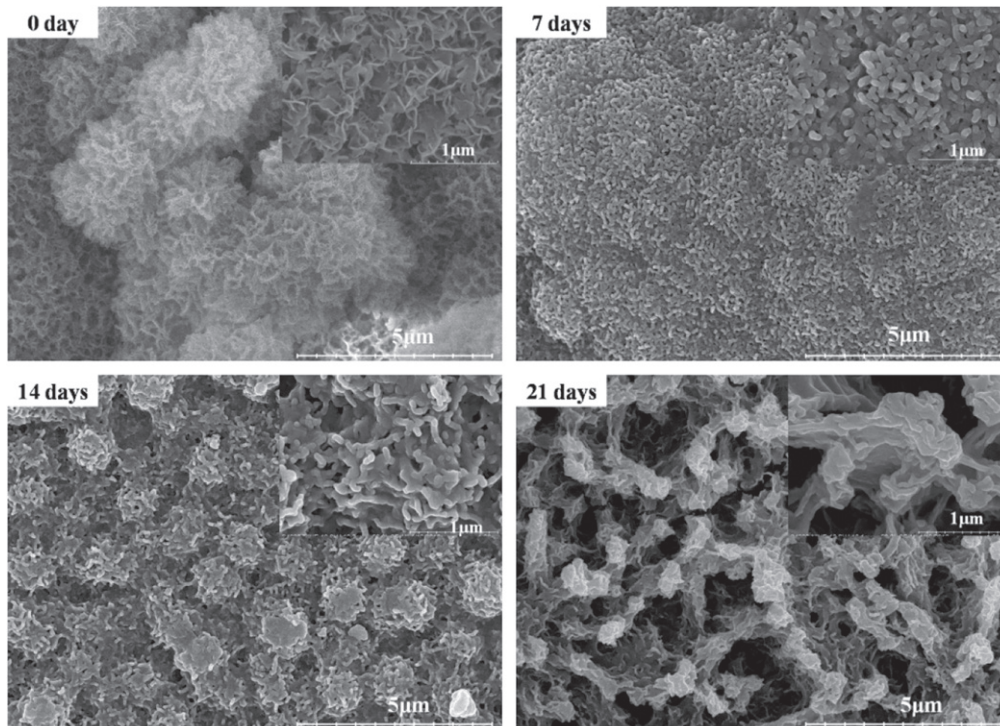


Figure 8. SEM images of Ti6Al4V before and after 21 immersion days in the SBF solution.



**Figure 9.** SEM images of HAp/Ti6Al4V samples before and after different immersion times in the SBF solution.

**Table 6.** Variation of  $E_{corr}$ ,  $i_{corr}$ ,  $R_p$  of Ti6Al4V and HAp/Ti6Al4V in the SBF solution versus the immersion times.

Time (day)	Ti6Al4V			HAp/Ti6Al4V		
	$E_{corr}$ (V/SCE)	$i_{corr}$ ( $\mu$ A)	$R_p$ (k $\Omega$ )	$E_{corr}$ (V/SCE)	$i_{corr}$ ( $\mu$ A)	$R_p$ (k $\Omega$ )
1	-0.136	1.25	11.4	-0.187	0.19	60.7
5	-0.107	0.64	22.4	-0.183	0.33	36.0
7	-0.121	0.76	18.8	-0.164	0.39	30.7
11	-0.125	1.19	12.0	-0.094	0.56	21.4
14	-0.137	0.99	14.4	-0.096	0.70	17.1
21	-0.153	0.90	15.9	-0.169	0.23	51.1

and 11.4 k $\Omega$ , respectively). This result shows that HAp coatings are capable to protect the substrate. The increase or the decrease of  $R_p$  shows the formation or the dissolution of HAp in the SBF solution. Generally, during immersion times the corrosion current density of substrate is higher than the one of sample covered by HAp coatings. The polarization resistance of substrate is lower than that of substrate covered by HAp. These results could indicate that the HAp coatings protect the substrate.

#### 4. Conclusion

HAp coatings have been successfully synthesized on the surface of Ti6Al4V by the electrodeposition method via a simple technique. The analysis results show that the HAp coatings were single phase crystals of HAp. HAp coatings have flake-

like shape to form coarse granular agglomerates. The *in vitro* test with Ti6Al4V and HAp/Ti6Al4V in the SBF solution were realized with different immersion times. SEM images showed the formation of apatite on the surface of Ti6Al4V and HAp/Ti6Al4V during the immersion time in the SBF solution. The apatite crystals had a cactus-like shape and covered fully the surface of HAp/Ti6Al4V material after 21 immersion days. The electrochemical behavior of Ti6Al4V and HAp/Ti6Al4V in the SBF solution shows the formation of apatite and HAp coatings behave as substrate protective layer.

#### Acknowledgments

This work was supported by Vietnam Academy of Science and Technology (under grant no. VAST. HTQT. FRANCE. 03/15-16) and was conducted within the context of the International Associated Laboratory ‘Functional Composite Materials’ (LIA-FOCOMAT) created between the ITT (Vietnam)-VAST and the CIRIMAT (France)-CNRS institutes.

#### References

- [1] Vasilescu C, Drob P, Vasilescu E, Demetrescu I, Ionita D, Prodana M and Drob S I 2011 *Corros. Sci.* **53** 992
- [2] Popa M V, Moreno J M C, Popa M, Vasilescu E, Drob P, Vasilescu C and Drob S I 2011 *Surf. Coat. Technol.* **205** 4776
- [3] Albayrak O, El-Atwani O and Altintas S 2008 *Surf. Coat. Technol.* **202** 2482
- [4] Kumar R M, Kishor K K, Sanjay S, Pallavi G, Bharat B, Gopinath P and Debrupa L 2016 *Surf. Coat. Technol.* **287** 82

- [5] Morks M F and Kobayashi A 2007 *Appl. Surf. Sci.* **253** 7136
- [6] Yung C Y and Chyun Y Y 2013 *Ceram. Int.* **39** 6509
- [7] Weng W and Baptista J L 1999 *J. Am. Ceram. Soc.* **82** 27
- [8] Balamurugan A, Kannan S and Rajeswari S 2002 *Trends Biomater. Artif. Organ.* **16** 18
- [9] Yang G L, He F M, Hu J A, Wang X X and Zhao S F 2009 *Oral Surg. Oral Med. Oral Pathol. Oral Radiol. Endod.* **107** 782
- [10] Gopi D, El-Sayed M S, Rajeswari D, Kavitha L, Pramod R, Jishnu D and Polaki S R 2014 *J. Alloys Compd.* **616** 498
- [11] Mrksich M and Whitesides G M 1996 *Annu. Rev. Biophys. Biomol. Struct.* **25** 55
- [12] Hallab N J, Mikecz K, Vermes C, Skipor A and Jacobs J J 2001 *J. Biomed. Mater. Res.* **56** 427
- [13] Zhao X, Yang L, Zuo Y and Xiong J 2009 *Chin. J. Chem. Eng.* **17** 667
- [14] Ugur T and Mustafa G 2010 *Ceram. Inter.* **36** 1805
- [15] Thanh D T M, Nam P T, Phuong N T, Que L X, Anh N V, Hoang T and Lam T D 2013 *Mater. Sci. Eng. C* **33** 2037
- [16] Xin F, Jian C, Jian-peng Z, QianW, Zhong-cheng Z and Jian-ming R 2009 *Trans. Nonferr. Met. Soc. China* **19** 347
- [17] Lin D Y and Wang X X 2010 *Surf. Coat. Technol.* **204** 3205
- [18] Myriam N, Olivier D, Oscar R M and Bernard T 2007 *J. Electroanal. Chem.* **600** 87
- [19] Alves V A, Reis R Q, Santos I C B, Souza D G, Goncalves T F, Pereira da Silva M A, Rossi A and Silva L A 2009 *Corros. Sci.* **51** 2473
- [20] Nath S, Tu R and Goto T 2011 *Surf. Coat. Technol.* **206** 172
- [21] Fleet M E 2009 *Biomaterials* **30** 1473